

# Recollision of excited electron in below-threshold nonsequential double ionization

**Xiaolei Hao**

Shanxi University <https://orcid.org/0000-0002-6049-2962>

**Yuxing Bai**

Shanxi University

**Chan Li**

Shanxi University

**Jingyu Zhang**

Shanxi University

**Weidong Li**

Shanxi University

**Weifeng Yang**

Shantou University <https://orcid.org/0000-0001-7451-9081>

**Mingqing Liu**

Institute of Applied Physics and Computational Mathematics

**Jing Chen** (✉ [chen\\_jing@iapcm.ac.cn](mailto:chen_jing@iapcm.ac.cn))

Institute of Applied Physics and Computational Mathematics

---

## Article

### Keywords:

**Posted Date:** September 2nd, 2021

**DOI:** <https://doi.org/10.21203/rs.3.rs-849385/v1>

**License:**   This work is licensed under a Creative Commons Attribution 4.0 International License.

[Read Full License](#)

---

**Version of Record:** A version of this preprint was published at Communications Physics on January 28th, 2022. See the published version at <https://doi.org/10.1038/s42005-022-00809-2>.

## **Title**

Recollision of excited electron in below-threshold nonsequential double ionization

## **Authors**

Xiaolei Hao<sup>1</sup>, Yuxing Bai<sup>1</sup>, Chan Li<sup>1</sup>, Jingyu Zhang<sup>1</sup>, Weidong Li<sup>2</sup>, Weifeng Yang<sup>3,\*</sup>, Mingqing Liu<sup>4</sup>, Jing Chen<sup>2,4,\*</sup>

## **Affiliations**

<sup>1</sup>Institute of Theoretical Physics and Department of Physics, State Key Laboratory of Quantum Optics and Quantum Optics Devices, Collaborative Innovation Center of Extreme Optics, Shanxi University, Taiyuan 030006, China.

<sup>2</sup>Shenzhen Key Laboratory of Ultraintense Laser and Advanced Material Technology, Center for Advanced Material Diagnostic Technology, and College of Engineering Physics, Shenzhen Technology University, Shenzhen 518118, China.

<sup>3</sup>School of Science, Hainan University, Hainan 570288, China.

<sup>4</sup>Institute of Applied Physics and Computational Mathematics, P. O. Box 8009, Beijing 100088, China.

\*Corresponding author. Email: wfyang@stu.edu.cn; chen\_jing@iapcm.ac.cn

## **Abstract**

Consensus has been reached that recollision, as the most important post-tunneling process, is responsible for nonsequential double ionization process in intense infrared laser field, however, its effect has been restricted to interaction between the first ionized electron and the residual ion so far. Here we identify the key role of recollision of the second ionized electron, which is enhanced by the stronger Coulomb potential of the higher valence residual ion, in the below-threshold nonsequential double ionization process by introducing a Coulomb-corrected quantum-trajectories method, which enables us to well reproduce the experimentally observed cross-shaped and anti-correlated patterns in correlated two-electron momentum distributions, and also the transition between these two patterns. Being significantly enhanced relatively by the recapture process which is also attributed to the stronger Coulomb potential of the residual ion, recolliding trajectories of the second electron excited by the first- or third-return recolliding trajectories of the first electron produce the cross-shaped or anti-correlated distributions, respectively. And the transition is induced by the increasing contribution of the third return with increasing pulse duration. Our work provides a new insight into atomic ionization dynamics and paves the new way to imaging of ultrafast dynamics of atoms and molecules in intense laser field.

## **Introduction**

Post-ionization process has been the focus of strong-field atomic and molecular physics in the past thirty years. A semiclassical perspective, in which the recollision process plays a key role, is established with great effort. It can well explain many intriguing strong-field phenomena, such as high-order above-threshold ionization (HATI), high harmonics generation (HHG), and nonsequential double ionization (NSDI), and also serves as the foundation of attosecond physics (see, e.g., Refs. (1-4) for reviews and references therein). In the recollision picture (5, 6), an electron is liberated from the neutral atom or molecule through tunneling, then is driven back by the laser field to collide with the parent ion elastically or inelastically, or recombine with the ion, resulting in HATI, NSDI and HHG, respectively. Since the electron strongly interacts with the ion, the products upon recollision carry information of the parent ion, and can be used to probe its structure and dynamics. Based on the recollision process, different methods, such as laser-induced electron diffraction (LIED) (7) and laser-induced electron inelastic diffraction (LIID) (8), are proposed and successfully applied in imaging of atomic and molecular ultrafast dynamics and

51 structure with unprecedented spatial-temporal resolution (8-15). However, the recollision in the  
52 above-mentioned strong-field processes and ultrafast imaging methods is limited to interaction  
53 between the first ionized electron and the residual ion.

54 In the NSDI process, one electron ( $e_1$ ) firstly experiences a recollision with the parent  
55 univalent ion and deliver energy to the bounded electron ( $e_2$ ). In the below-threshold regime, the  
56 maximal kinetic energy of  $e_1$  upon recollision is smaller than the ionization potential of  $e_2$ , so  $e_2$   
57 can be only pumped to an excited state, as illustrated in Fig. 1. Then  $e_2$  is ionized from the excited  
58 state by the laser field at a later time, dubbed as recollision excitation with subsequent ionization  
59 (RESI) process. Usually, it is believed that  $e_2$  will travel directly to the detector (16-19), i. e., the  
60 post-tunneling process of  $e_2$  has been largely ignored. In fact, after tunneling ionization,  $e_2$  may be  
61 driven back to recollide with the divalent ion or be recaptured into a Rydberg state of ion as  
62 illustrated in Fig. 1. Due to the strong Coulomb field of the divalent ion, these post-tunneling  
63 dynamics may be prominent. It has been recently reported experimentally and theoretically that  
64 the probability of recapture in double ionization, dubbed as frustrated double ionization (FDI), is  
65 much higher than expectation (20, 21).

66 In this work, by introducing a Coulomb-corrected quantum-trajectories (CCQT) method, we  
67 identify the key role played by the recollision between the second ionized electron and the  
68 divalent ion in the below-threshold NSDI process. We find that, only when this recollision is  
69 included, the experimentally observed cross-shaped (22, 23) and anti-correlated (24) patterns of  
70 correlated electron momentum distribution (CEMD), and also the transition between them (25),  
71 can be well reproduced.

## 72 **Results**

### 73 **Comparison with experimental results**

74 Fig. 2 displays the calculated results for Ar under different pulse durations to compare with the  
75 experimental results in Ref. (25). Intensities higher than the measured ones by  $0.25 \times 10^{14}$  W/cm<sup>2</sup>  
76 are used in the present calculations (see Supplementary Materials for details of the fitting  
77 procedure). As shown in Fig. 2, for shorter pulse durations (4 fs and 8 fs), the distributions show a  
78 cross shape with the maxima lying at the origin. While for longer pulses (16 fs and 30 fs), the  
79 electrons are more homogeneously distributed over the four quadrants, actually, prefer the second  
80 and fourth quadrants, which indicates an anti-correlation. This transition of CEMD from cross-  
81 shaped to anti-correlated patterns is in agreement with the measured results reported in Ref. (25),  
82 although there is some discrepancy in details. In the measurement, the transition occurs when  
83 pulse duration increases from 4 fs to 8 fs, whereas in Fig. 2 it occurs when pulse duration  
84 increases from 8 fs to 16 fs. This discrepancy may be due to that the pulse shape and duration  
85 employed in our calculations are not exactly the same as that in the measurements.

86 To quantitatively characterize the CEMD, in Fig. 2c we plot the ratio  $Y_{2\&4}/Y_{1\&3}$  for different  
87 pulse durations and different intensities.  $Y_{1\&3}$  ( $Y_{2\&4}$ ) denotes the integrated yield in the first and  
88 third (the second and fourth) quadrants. We also present the measured results (25) in Fig. 2f for  
89 comparison. In general, the simulation reproduces most of the features in the measured results.  
90 The ratio increases with pulse duration and becomes saturated at 16 fs when the intensity is fixed,  
91 and it decreases with laser intensity both for pulse durations of 8 fs and 16 fs. However, compared  
92 with the measured results, the simulation obviously overestimates the ratio for the highest  
93 intensity. This discrepancy can be attributed to that the contribution of the process that  $e_2$  is  
94 directly knocked out by  $e_1$ , whose distribution mainly locates in the first and third quadrants,  
95 becomes more significant with increasing intensity, but is not included here.

### 96 **Recolliding trajectories of $e_2$**

97 In Fig. 3, we present CEMDs corresponding to recolliding trajectories and direct trajectories of  $e_2$   
98 at 4 fs and 30 fs, respectively. Here, we define it as the recolliding trajectory if the minimal  
99 distance of  $e_2$  from the residual ion is less than the tunnel exit. Otherwise, it is the direct trajectory.  
100

101 Since momenta of direct trajectories of  $e_2$  are much smaller than that of recolliding trajectories,  
 102 CEMDs for direct trajectories are localized around the origin for both 4 fs and 30 fs pulses, as  
 103 shown in Figs. 3A and 3D. Whereas the CEMD for recolliding trajectories exhibits a cross  
 104 structure at 4 fs (Fig. 3b), and exhibits an anti-correlated pattern at 30 fs (Fig. 3e). Meanwhile,  
 105 recolliding trajectories of  $e_2$  have dominant contributions for all pulse durations as depicted by the  
 106 ratio  $Y_{\text{res}}/Y_{\text{dir}}$  ( $Y_{\text{res}}$  and  $Y_{\text{dir}}$  denote the yields of recolliding and direct trajectories, respectively) for  
 107 double ionization (DI) events in Fig. 3c, as a consequence, the total CEMDs also shows a cross or  
 108 an anti-correlated pattern at 4 fs or 30 fs, respectively.

109 But why the relative contribution of the recolliding trajectories of  $e_2$  is so high? Intuitively,  
 110 the Coulomb focusing effect imposed on  $e_2$  by the divalent cation, which is much stronger than  
 111 that of the univalent cation in ATI process, will effectively enhance the probability of recollision.  
 112 We can indeed see this clearly from Fig. 3c in which the ratio  $Y_{\text{res}}/Y_{\text{dir}}$  with all events included is  
 113 greater than 1. But it is still much smaller than the ratio considering only DI events. This  
 114 deviation is the result of the important contribution of recapture or FDI process. More than two-  
 115 thirds of direct  $e_2$  are recaptured into the Rydberg states of  $\text{Ar}^+$  at 4fs, and the probability of FDI  
 116 for direct  $e_2$  decreases quickly with increasing pulse duration, as shown in Fig. 3f. Compared with  
 117 recolliding trajectory of  $e_2$ , direct  $e_2$  cannot move far away from  $\text{Ar}^{2+}$  at the end of the pulse due  
 118 to its much lower momentum, especially in shorter laser pulse, therefore is easier to be recaptured  
 119 by the strong Coulomb field of the divalent ion. More direct  $e_2$  being recaptured means fewer of  
 120 them contribute to DI, resulting in larger relative contribution of recolliding trajectories of  $e_2$  to  
 121 DI. In brief, the enhanced FDI probability significantly enlarges the relative contribution of  
 122 recolliding trajectories of  $e_2$  to DI, and eventually induces the experimentally observed cross-  
 123 shaped and anti-correlated patterns. In addition, this point is strongly supported by the fact that  
 124 when only the direct trajectories of  $e_2$  are considered, the calculated  $Y_{2\&4}/Y_{1\&3}$  is significantly  
 125 different from the experimental result (see Fig. 2c).

### 126 **Transition of CEMD with increasing pulse duration**

127 The specific pattern of CEMD also requires the appropriate momentum of  $e_1$  which is determined  
 128 by the microscopic dynamics of the recollision process for  $e_1$ . According to our calculations, the  
 129 first- and third-return recolliding trajectories of  $e_1$  are dominant for the laser parameters interested  
 130 here. For other returns, either the return energy is too small to excite  $e_2$ , or the collision  
 131 probability is negligible due to the spreading of the wave packet. In Figs. 4A and 4B, we present  
 132 the CEMDs corresponding to the first- and third-return trajectories of  $e_1$ , respectively, in  
 133  $1.25 \times 10^{14}$  W/cm<sup>2</sup>, 30 fs laser pulse. Note that all trajectories of  $e_2$  (direct and recolliding  
 134 trajectories) are included. The CEMD for the first-return trajectories of  $e_1$  (Fig. 4a) shows a cross-  
 135 shaped pattern, whereas that for the third-return trajectories (Fig. 4b) exhibits an anti-correlated  
 136 pattern. As shown in Fig. 4c, the ratio of the integrated yield of the third-return trajectories to that  
 137 of the first-return increases quickly with increasing pulse duration. Correspondingly, the CEMD  
 138 changes from a cross-shaped to an anti-correlated pattern. Therefore, the transition between the  
 139 two patterns of CEMD with increasing pulse duration is the result of increasing contribution of  
 140 the third-return trajectories of  $e_1$ . The significant contribution of the third-return trajectories can  
 141 be attributed to the Coulomb focusing effect from the univalent cation. The similar effect has also  
 142 been reported for high-order ATI process (32).

### 143 **Cross-shaped and anti-correlated CEMDs**

144 Next, we will explain how the cross-shaped and anti-correlated patterns of CEMDs are formed by  
 145 the recolliding trajectories of the two electrons. Without indistinguishability symmetrization, the  
 146 first-return trajectories of  $e_1$  will show a band-like distribution along the  $p_{1z}=0$  axis with the  
 147 maxima away from the origin, i. e., vanishing momentum of  $e_1$  but much higher momentum of  $e_2$   
 148 (Fig. 5b). Whereas the CEMD for the third-return consists of two bands and the maximum of the  
 149 left (right) band lies in the up (low) part, giving rise to an anti-correlation (Fig. 5c). These band-  
 150 like distributions can be understood as follows. The final momentum of  $e_1$  is determined by the

151 residual momentum after exciting  $e_2$  and the drift momentum it obtains from the laser field. Since  
 152 forward scattering is favored in this inelastic scattering process, the residual momentum and the  
 153 drift momentum are in opposite directions and will cancel with each other. At the present  
 154 intensity ( $1.25 \times 10^{14}$  W/cm<sup>2</sup>), the magnitudes of them for the first-return trajectories of  $e_1$  are  
 155 nearly equal, resulting in a vanishing momentum of  $e_1$ . When the laser intensity increases, the  
 156 band will become tilted towards the main diagonal (23) due to the faster-increasing residual  
 157 momentum. For the third-return, its return energy is smaller than that of the first-return, so the  
 158 residual momentum is not enough to compensate the drift momentum, resulting in a non-  
 159 vanishing momentum of  $e_1$ . Since electrons ionized at times separated by a half optical cycle will  
 160 have opposite momenta, there is one band on each side of  $p_{1z}=0$  axis. Actually, there are also two  
 161 bands for the first return, but they merge together.

162 The anti-correlation between the two electrons for the third-return trajectories of  $e_1$  is  
 163 illustrated in Fig. 5a. The recollision of  $e_1$  most probably occurs around the crossing of the  
 164 electric field at  $t_{1r}$  or  $t'_{1r}$ . Since the magnitude of the drift momentum after recollision, which is  
 165 equal to  $-\mathbf{A}(t_{1r})$  (vector potential at the recollision time), is larger than the residual momentum  
 166 for the third-return recolliding trajectories of  $e_1$ , its final momentum is in the direction of the drift  
 167 momentum. If the recollision of  $e_1$  occurs at  $t_{1r}$ , the final momentum of  $e_1$  will be positive,  
 168 corresponding to the right band in Fig. 5c. Upon recollision,  $e_2$  is pumped to the first excited state,  
 169 then it is most probably ionized at the subsequent electric field peak at  $t_{2i}$ . If the Coulomb  
 170 attraction of the ion is not considered and no recollision occurs,  $e_2$  will have vanishing final  
 171 momentum. This can be seen clearly in Figs. 5D and 5E, in which the CEMDs are obtained by  
 172 calculating  $M_{\mathbf{p}_2}^{(3)}$  in Eq. (1) (see the Materials and Methods) with the standard SFA. But if the  
 173 ionic Coulomb potential is taken into account, momenta of  $e_2$  for recolliding trajectories  
 174 (trajectory I) shift to the negative direction, opposite to the direction of the final momentum of  $e_1$   
 175 (see Fig. 5a). This is exactly the situation of the right-band distribution in Fig. 5c. The left band  
 176 corresponds to the situation that  $e_1$  recollides with the ion at  $t'_{1r}$  and  $e_2$  is ionized at  $t'_{2i}$ . As a  
 177 consequence, the two electrons are emitted back-to back and the CEMD exhibits an anti-  
 178 correlated pattern. In addition, it is also possible that the recollision of  $e_1$  occurs at  $t_{1r}$  while  $e_2$  is  
 179 ionized at  $t'_{2i}$ , which will produce a correlated CEMD. But since its contribution is smaller due to  
 180 the depletion effect of the excited state, the total CEMD will still exhibit an anti-correlated  
 181 pattern.

### 182 **Prediction for higher valence ions**

183 It is expected that the effect of the Coulomb field for higher valence ion will be stronger. This can  
 184 be demonstrated in the DI process of Ar<sup>+</sup>. As shown in Fig. 6a, the recollision probability of  $e_2$   
 185 in the presence of the Coulomb field of Ar<sup>3+</sup> is higher than that for Ar<sup>2+</sup> shown in Fig. 2e. The  
 186 CEMD also exhibits a strong dependence on the laser intensity and pulse duration. A similar to  
 187 Fig. 2a but more obvious cross structure appears in the CEMD for laser field of 400 nm with  
 188 pulse duration of 4fs and intensity of  $4 \times 10^{14}$  W/cm<sup>2</sup> (Fig. 6b) - the arms get thinner and longer.  
 189 When the laser intensity increases to  $8 \times 10^{14}$  W/cm<sup>2</sup> which is still lower than the threshold  
 190 intensity of  $8.6 \times 10^{14}$  W/cm<sup>2</sup>, the CEMD transits to a correlated pattern (Fig. 6c). If increasing the  
 191 pulse duration to 16 fs, the CEMD then transits back to the cross structure (Fig. 6d). It is the result  
 192 of increasing contribution of the third-return trajectories of  $e_1$  which just meets the requirements  
 193 of cross structure. It is noteworthy that, for convenience of experimental observation, we employ  
 194 400 nm laser pulses in the above calculations for NSDI of Ar<sup>+</sup> which enable us to apply higher  
 195 laser intensity to obtain higher ionization probability but remains in the below-threshold region.  
 196 The additional complexity in experimental aspect comes from preparing Ar<sup>+</sup> instead of Ar atoms  
 197 as targets, but it should not be an impossible task under current experimental conditions (33).

## 199 Discussion

200 We propose a Coulomb-corrected quantum-trajectories (CCQT) method to describe the below-  
 201 threshold NSDI process both coherently and quantitatively. It enables us to well reproduce  
 202 different kinds of CEMDs observed in experiments, and uncover the rich underlying physics  
 203 induced by the Coulomb field of univalent, divalent and higher valence ions, including the multi-  
 204 return trajectories of the first ionized electron  $e_1$ , the recollision and recapture processes of the  
 205 second ionized electron  $e_2$ . Especially, recollision process of  $e_2$ , which is enhanced relatively by  
 206 the recapture process of  $e_2$ , is found to play an important role in electron-electron correlation. We  
 207 expect that the recollision process of  $e_2$  can be applied to develop a new scheme to image the  
 208 ultrafast evolution of the molecular structure and dynamics induced by the strong laser field.

209

## 210 Materials and Methods

211 To describe the below-threshold NDSI process both coherently and quantitatively, it has to  
 212 incorporate both the quantum effect and the Coulomb interaction between the residual ion and the  
 213 ionized electrons in a uniform theory. To achieve this, we introduce a Coulomb-corrected  
 214 quantum-trajectories (CCQT) method by taking advantage of the well-developed Coulomb-  
 215 corrected methods dealing with single-electron dynamics. The transition magnitude is expressed  
 216 as (atomic units  $m = \hbar = e = 1$  are used)

$$217 \quad M\left(\tilde{\mathbf{P}}_1, \tilde{\mathbf{P}}_2\right) = \sum_s M_{\tilde{\mathbf{P}}_2}^{(3)}\left(t_{2i}^s, t_{1r}^s\right) M_{\tilde{\mathbf{P}}_1}^{(2)}\left(t_{1r}^s\right) M_{\tilde{\mathbf{P}}_1}^{(1)}\left(t_{1r}^s, t_{1i}^s\right) \quad (1)$$

218 in which different trajectories labelled with  $s$  are summed coherently.  $M_{\tilde{\mathbf{P}}_1}^{(1)}\left(t_{1r}^s, t_{1i}^s\right)$ , describing the

219 tunneling ionization of  $e_1$  at  $t_{1i}^s$  and its subsequent propagation in the laser field until colliding  
 220 with the parent ion at time  $t_{1r}^s$ , is calculated using the quantum-trajectory Monte Carlo (QTMC)  
 221 method (26,27) which is efficient to obtain large amount of hard-collision trajectories.  
 222 Trajectories with minimum distance from the ion less than 1 a.u. are selected to consider the hard  
 223 collision for the subsequent calculation. Upon collision,  $e_1$  will excite  $e_2$  and then move to the  
 224 detector. This excitation process is described by  $M_{\tilde{\mathbf{P}}_1}^{(2)}\left(t_{1r}^s\right)$  which is calculated with conventional

225 S-matrix theory. Finally,  $e_2$  is ionized through tunneling at  $t_{2i}^s$  from the excited state, and then  
 226 propagates in the laser field until the end of the pulse, which is described by  $M_{\tilde{\mathbf{P}}_2}^{(3)}\left(t_{2i}^s, t_{1r}^s\right)$

227 calculated with the Coulomb-corrected strong field approximation (CCSFA) method (28). The  
 228 sin-squared pulse shape is employed in our calculation. A model potential (29) is applied to  
 229 mimic the Coulomb field of  $\text{Ar}^{2+}$  felt by  $e_2$  in its propagation. Only the first excited state  $3s3p6$   
 230 with zero magnetic quantum number (30) is included in the present calculations. The depletion of  
 231 the excited state is also taken into account in calculating  $M_{\tilde{\mathbf{P}}_2}^{(3)}\left(t_{2i}^s, t_{1r}^s\right)$  (18) (see the method in

232 Supplementary Materials).

233

234 **Data availability:** All data are available in the main text or the supplementary materials.

## References

1. M. Protopapas, C. H. Keitel, P. L. Knight, Atomic physics with super-high intensity lasers, *Rep. Prog. Phys.* **60**, 389-486 (1997).
2. W. Becker, F. Grasbon, R. Kopold, D. B. Milošević, G. G. Paulus, H. Walther, Above-threshold ionization: from classical features to quantum effects, *Adv. At. Mol. Opt. Phys.* **48**, 35-98 (2002).
3. W. Becker, X. J. Liu, P. J. Ho, J. H. Eberly, Theories of photoelectron correlation in laser-driven multiple atomic ionization, *Rev. Mod. Phys.* **84**, 1011-1043(2012).
4. F. Krausz, M. Ivanov, Attosecond physics, *Rev. Mod. Phys.* **81**, 163-234 (2009).
5. P. B. Corkum, Plasma perspective on strong-field multiphoton ionization, *Phys. Rev. Lett.* **71**, 1994-1997 (1993).
6. K. J. Schafer, Baorui Yang, L. F. DiMauro, K. C. Kulander, Above threshold ionization beyond the high harmonic cutoff, *Phys. Rev. Lett.* **70**, 1599-1602 (1993).
7. T. Morishita, A.-T. Le, Z. Chen, C. D. Lin, Accurate retrieval of structural information from laser-induced photoelectron and high-order harmonic spectra by few-cycle laser pulses, *Phys. Rev. Lett.* **100**, 013903 (2008).
8. W. Quan, X. L. Hao, X. Q. Hu, R. P. Sun, Y. L. Wang, Y. J. Chen, S. G. Yu, S. P. Xu, Z. L. Xiao, X. Y. Lai, X. Y. Li, W. Becker, Y. Wu, J. G. Wang, X. J. Liu, J. Chen, Laser-induced inelastic diffraction from strong-field double ionization, *Phys. Rev. Lett.* **119**, 243203 (2017).
9. M. Okunishi, T. Morishita, G. Prümper, K. Shimada, C. D. Lin, S. Watanabe, K. Ueda, Experimental retrieval of target structure information from laser-induced rescattered photoelectron momentum distributions, *Phys. Rev. Lett.* **100**, 143001 (2008).
10. D. Ray, B. Ulrich, I. Bocharova, C. Maharjan, P. Ranitovic, B. Gramkow, M. Magrakvelidze, S. De, I. V. Litvinyuk, A.-T. Le, T. Morishita, C. D. Lin, G. G. Paulus, C. L. Cocke, Large-angle electron diffraction structure in laser-induced rescattering from rare gases, *Phys. Rev. Lett.* **100**, 143002 (2008).
11. M. Meckel, D. Comtois, D. Zeidler, A. Staudte, D. Pavičić, H. C. Bandulet, H. Pépin, J. C. Kieffer, R. Dörner, D. M. Villeneuve, P. B. Corkum, Laser-induced electron tunneling and diffraction, *Science* **320**, 1478-1482 (2008).
12. C. I. Bлага, J. Xu, A. D. DiChiara, E. Sistrunk, K. Zhang, P. Agostini, T. A. Miller, L. F. DiMauro, C. D. Lin, Imaging ultrafast molecular dynamics with laser-induced electron diffraction, *Nature* **483**, 194-197 (2012).
13. H. Niikura, F. Légaré, R. Hasbani, A. D. Bandrauk, M. Y. Ivanov, D. M. Villeneuve, P. B. Corkum, Controlling electron-ion-recollision dynamics with attosecond precision, *Nature* **417**, 917-922 (2002).
14. J. Itatani, J. Levesque, D. Zeidler, H. Niikura, H. Pépin, J. C. Kieffer, P. B. Corkum, D. M. Villeneuve, Tomographic imaging of molecular orbitals, *Nature* **432**, 867-871 (2004).
15. B. Wolter, M. G. Pullen, A.-T. Le, M. Baudisch, K. Doblhoff-Dier, A. Senftleben, M. Hemmer, C. D. Schröter, J. Ullrich, T. Pfeifer, R. Moshhammer, S. Gräfe, O. Vendrell, C. D. Lin, J. Biegert, Ultrafast, electron diffraction imaging of bond breaking in di-ionized acetylene, *Science* **354**, 308-312 (2016).
16. T. Shaaran, M. T. Nygren, C. Figueira de Morisson Faria, Laser-induced nonsequential double ionization at and above the recollision-excitation-tunneling threshold, *Phys. Rev. A* **81**, 063413 (2010).
17. B. Wang, Y. Guo, J. Chen, Z. Yan, P. Fu, Frequency-domain theory of nonsequential double ionization in intense laser fields based on nonperturbative QED, *Phys. Rev. A* **85**, 023402 (2012).
18. X. L. Hao, J. Chen, W. D. Li, B. Wang, X. Wang, W. Becker, Quantum effects in double ionization of Argon below the threshold intensity, *Phys. Rev. Lett.* **112**, 073002 (2014).
19. A. S. Maxwell, C. Figueira de Morisson Faria, Controlling below-threshold nonsequential double ionization via quantum interference, *Phys. Rev. Lett.* **116**, 143001 (2016).

- 285 20. S. Larimian, S. Erattupuzha, A. Baltuška, M. Kitzler-Zeiler, X. Xie, Frustrated double  
286 ionization of argon atoms in strong laser fields, *Phys. Rev. Research* **2**, 013021 (2020).
- 287 21. S. Chen, J. Chen, G. G. Paulus, H. Kang, Strong-field frustrated double ionization of argon  
288 atoms, *Phys. Rev. A* **102**, 023103 (2020).
- 289 22. B. Bergues, M. Kübel, N. Johnson, B. Fischer, N. Camus, K. Betsch, O. Herrwerth, A.  
290 Senftleben, A. Saylor, T. Rathje, T. Pfeifer, I. Ben-Itzhak, R. Jones, G. Paulus, F. Krausz, R.  
291 Moshhammer, J. Ullrich, M. Kling, Attosecond tracing of correlated electron-emission in non-  
292 sequential double ionization, *Nat. Commun.* **3**, 813 (2012).
- 293 23. M. Kübel, C. Burger, N. G. Kling, T. Pischke, L. Beaufore, I. Ben-Itzhak, G. G. Paulus, J.  
294 Ullrich, T. Pfeifer, R. Moshhammer, M. F. Kling, B. Bergues, Complete characterization of single-  
295 cycle double ionization of argon from the nonsequential to the sequential ionization regime, *Phys.*  
296 *Rev. A* **93**, 053422 (2016).
- 297 24. Y. Liu, S. Tschuch, A. Rudenko, M. Dürr, M. Siegel, U. Morgner, R. Moshhammer, J. Ullrich,  
298 Strong-field double ionization of Ar below the recollision threshold, *Phys. Rev. Lett.* **101**, 053001  
299 (2008).
- 300 25. M. Kübel, K. J. Betsch, N. G. Kling, A. S. Alnaser, J. Schmidt, U. Kleineberg, Y. Deng, I.  
301 Ben-Itzhak, G. G. Paulus, T. Pfeifer, J. Ullrich, R. Moshhammer, M. F. Kling B. Bergues, Non-  
302 sequential double ionization of Ar: from the single- to the many-cycle regime, *New J. Phy.* **16**,  
303 033008 (2014).
- 304 26. M. Li, J. Geng, H. Liu, Y. Deng, C. Wu, L. Peng, Q. Gong, Y. Liu, Classical-quantum  
305 correspondence for above-threshold ionization, *Phys. Rev. Lett.* **112**, 113002 (2014).
- 306 27. X. Song, C. Lin, Z. Sheng, P. Liu, Z. Chen, W. Yang, S. Hu, C. D. Lin, J. Chen, Unraveling  
307 nonadiabatic ionization and Coulomb potential effect in strong-field photoelectron holography,  
308 *Sci. Rep.* **6**, 28392 (2016).
- 309 28. T. M. Yan, S. V. Popruzhenko, M. J. J. Vrakking, and D. Bauer, Low-energy structures in  
310 strong field ionization revealed by quantum orbits, *Phys. Rev. Lett.* **105**, 253002 (2010).
- 311 29. X. Tong, C. Lin, Empirical formula for static field ionization rates of atoms and molecules by  
312 lasers in the barrier-suppression regime, *J. Phys. B* **38**, 2593-2600 (2005).
- 313 30. K. G. Dyall, I. P. Grant, F. A. Parpia, E. P. Plummer, GRASP: A general-purpose relativistic  
314 atomic structure program, *Comput. Phys. Commun.* **55**, 425-456 (1989).
- 315 31. X. L. Hao, W. D. Li, J. Liu, J. Chen, Effect of the electron initial longitudinal velocity on the  
316 nonsequential double-ionization process, *Phys. Rev. A* **83**, 053422 (2011).
- 317 32. X. L. Hao, Y. X. Bai, X. Y. Zhao, C. Li, J. Y. Zhang, J. L. Wang, W. D. Li, C. L. Wang, W.  
318 Quan, X. J. Liu, Z. Shu, M. Liu, J. Chen, Effect of Coulomb field on laser-induced ultrafast  
319 imaging methods, *Phys. Rev. A* **101**, 051401(R) (2020).
- 320 33. J. B. Greenwood, I. M. G. Johnston, P. McKenna, I. D. Williams, T. R. J. Goodworth, J. H.  
321 Sanderson, W. A. Bryan, A. A. A. El-Zein, W. R. Newell, A. J. Langley E. J. Dival, Suppression  
322 of multiple ionization of atomic ions in intense ultrafast laser pulses, *Phys. Rev. Lett.* **88**, 233001  
323 (2002).

### 324 **Acknowledgments**

325 The calculations were performed on High Performance Computing System of Shanxi University.  
326 This work was partially supported by the National Key Program for S&T Research and  
327 Development (No. 2019YFA0307700), the National Natural Science Foundation of China (Grants  
328 No. 11874246, No. 91950101, No. 11774215).

### 329 **Author contributions**

330 X.H., W.Y., and J.C. designed the research; X.H. and Y.B. performed all the simulations; X.H.,  
331 Y.B., C.L., and J.Z. analyzed data; X.H., W.L., W.Y., and J.C. discussed the results; X.H., W.L.,

334 W.Y., and J.C. wrote the paper.

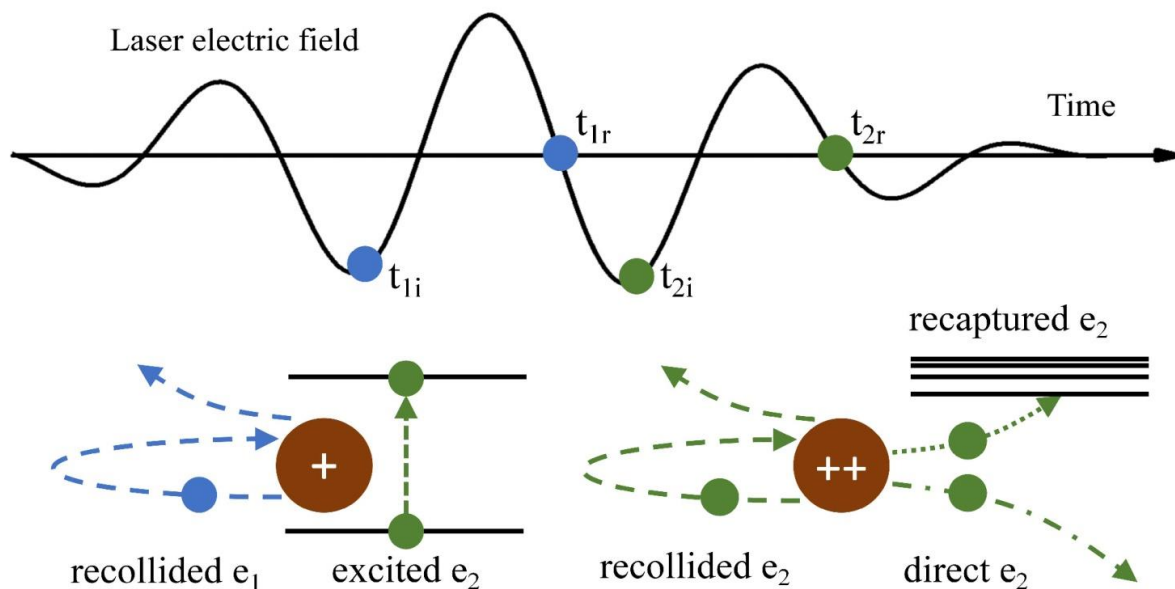
335

### 336 Competing interests

337 The authors declare no competing interests.

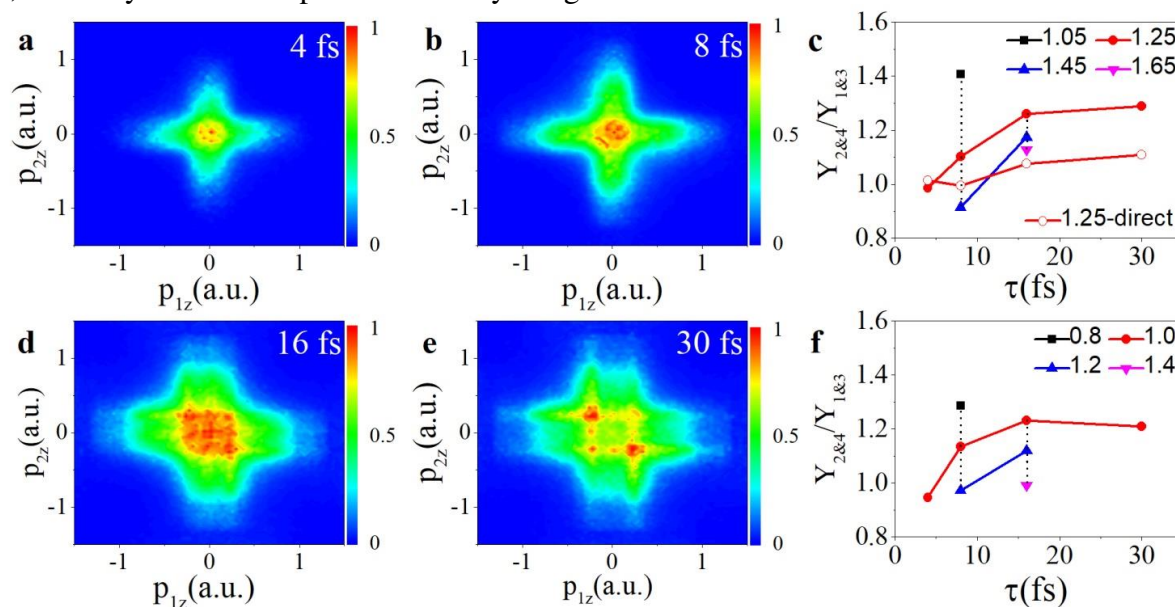
338

### 339 Figures



340

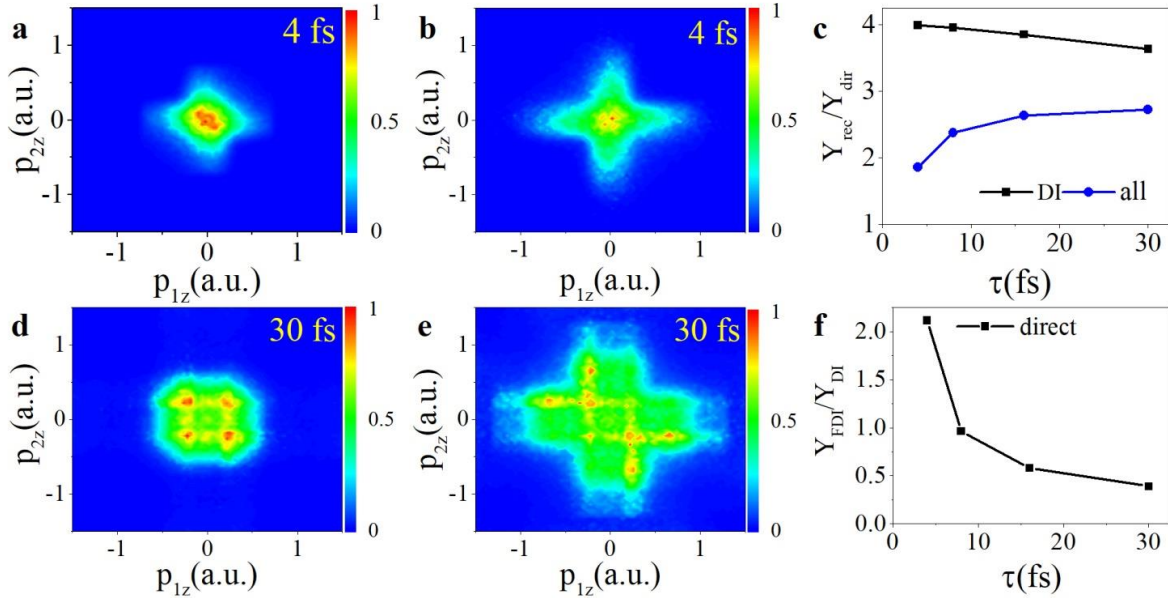
341 **Fig. 1. Sketch map to illustrate the below-threshold NSDI process.** At time  $t_{1i}$ ,  $e_1$  is first  
342 ionized by the laser field, then it is driven back to collide the parent univalent ion and excites  $e_2$   
343 at time  $t_{1r}$ .  $e_2$  is ionized from the excited state by the laser field at a later time  $t_{2i}$ . After that,  $e_2$  may  
344 travel directly to the detector, or it may be driven back to recollide with the divalent ion similar to  
345  $e_1$ , or it may also be recaptured into a Rydberg state of ion.



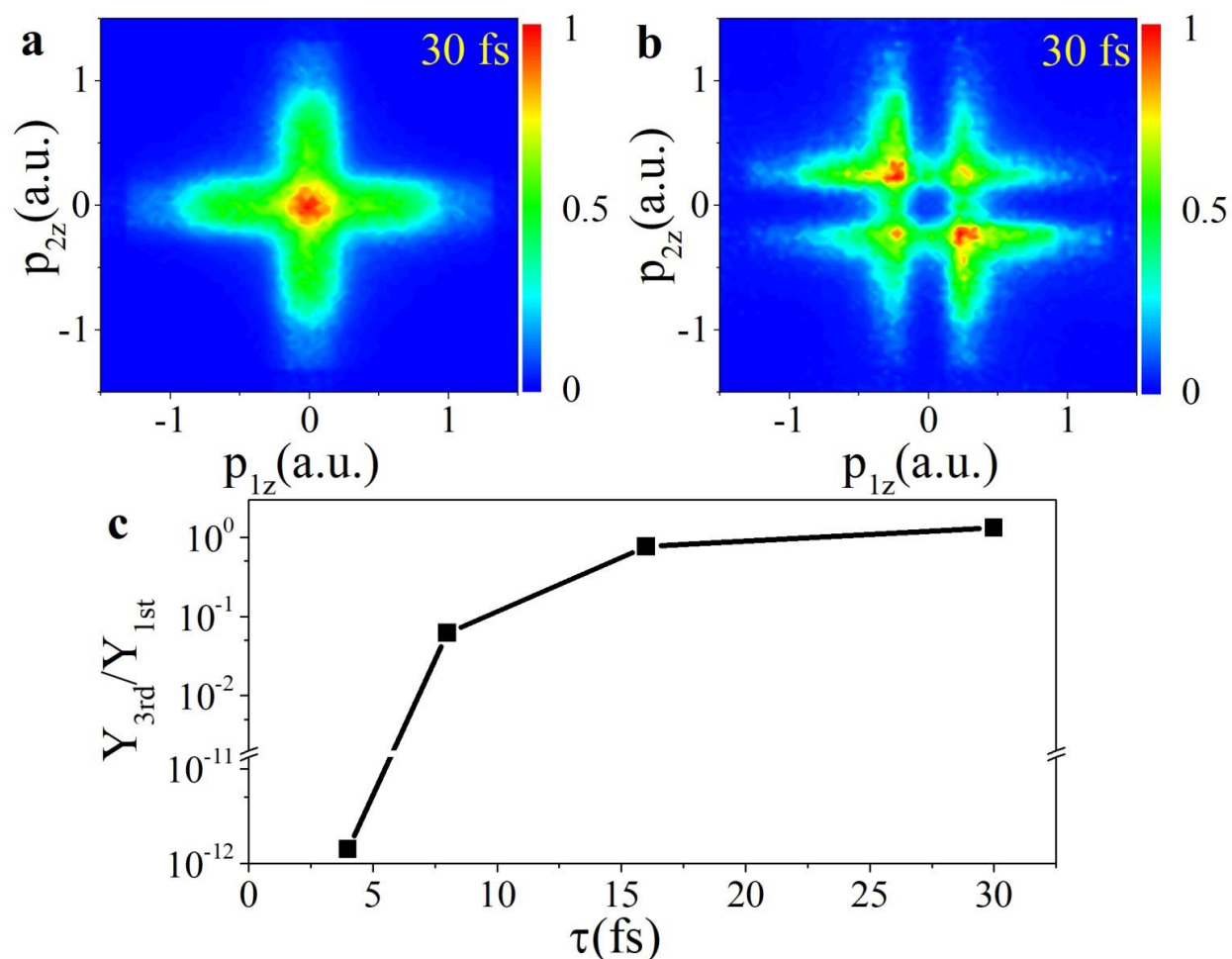
346

347 **Fig. 2. Simulated results for below-threshold NSDI of Ar.** (a), (b), (d) and (e) Simulated  
348 correlated electron momentum distributions (CEMDs) of Ar for different laser pulse durations at

349 the intensity of  $1.25 \times 10^{14}$  W/cm<sup>2</sup>. The CEPs are averaged. Each CEMD is normalized to itself. (c)  
 350 Simulated yield ratio  $Y_{2\&4}/Y_{1\&3}$  for different pulse durations and different intensities.  $Y_{1\&3}$  ( $Y_{2\&4}$ )  
 351 denotes the integrated yield in the first and third (the second and fourth) quadrants in the CEMD.  
 352 The numbers given in the legends denote peak laser intensities with units of  $10^{14}$  W/cm<sup>2</sup>. The  
 353 open circles are calculated by only considering direct trajectories of  $e_2$  (see text for details). (f)  
 354 Measured results extracted from Ref.[25]. The black short-dashed lines in (c) and (f) serve as  
 355 indications of the intensity dependence.

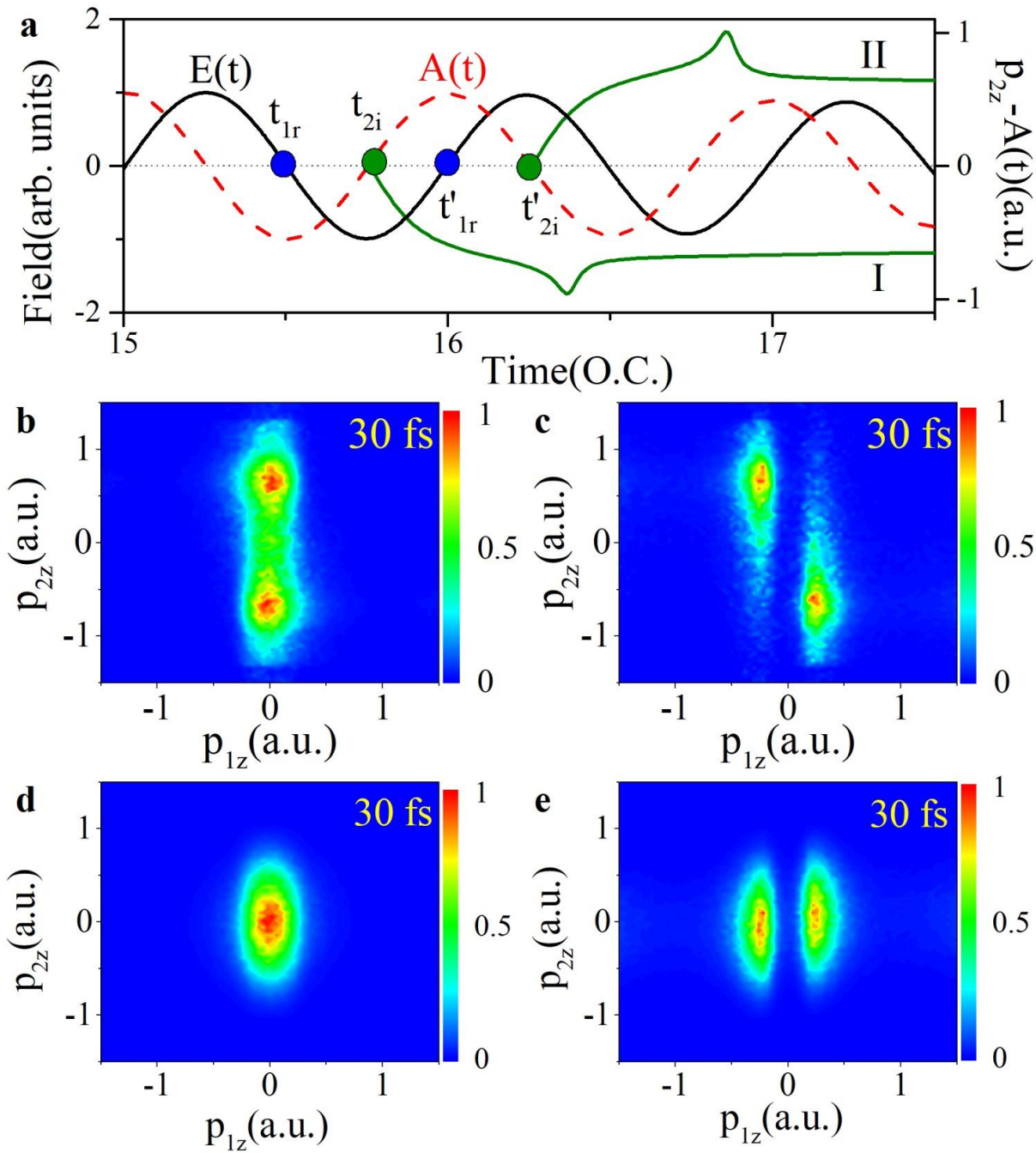


356 **Fig. 3. Distributions corresponding to recolliding trajectories and direct trajectories of  $e_2$ .** (a)  
 357 and (d) CEMDs corresponding to direct trajectories of  $e_2$ . (b) and (e) CEMDs corresponding to  
 358 recolliding trajectories of  $e_2$ . (c) Pulse-duration dependence of  $Y_{\text{rec}}/Y_{\text{dir}}$ , the ratio between the  
 359 integrated yields of recolliding and direct trajectories for  $e_2$  for all events or only double  
 360 ionization (DI) events. (f) Pulse-duration dependence of  $Y_{\text{FDI}}/Y_{\text{DI}}$ , the ratio between the  
 361 probabilities of FDI and DI when  $e_2$  is confined to direct trajectories. The laser intensity is  
 362  $1.25 \times 10^{14}$  W/cm<sup>2</sup>. Each CEMD is normalized to itself. The CEPs are averaged.



364  
365  
366  
367  
368  
369

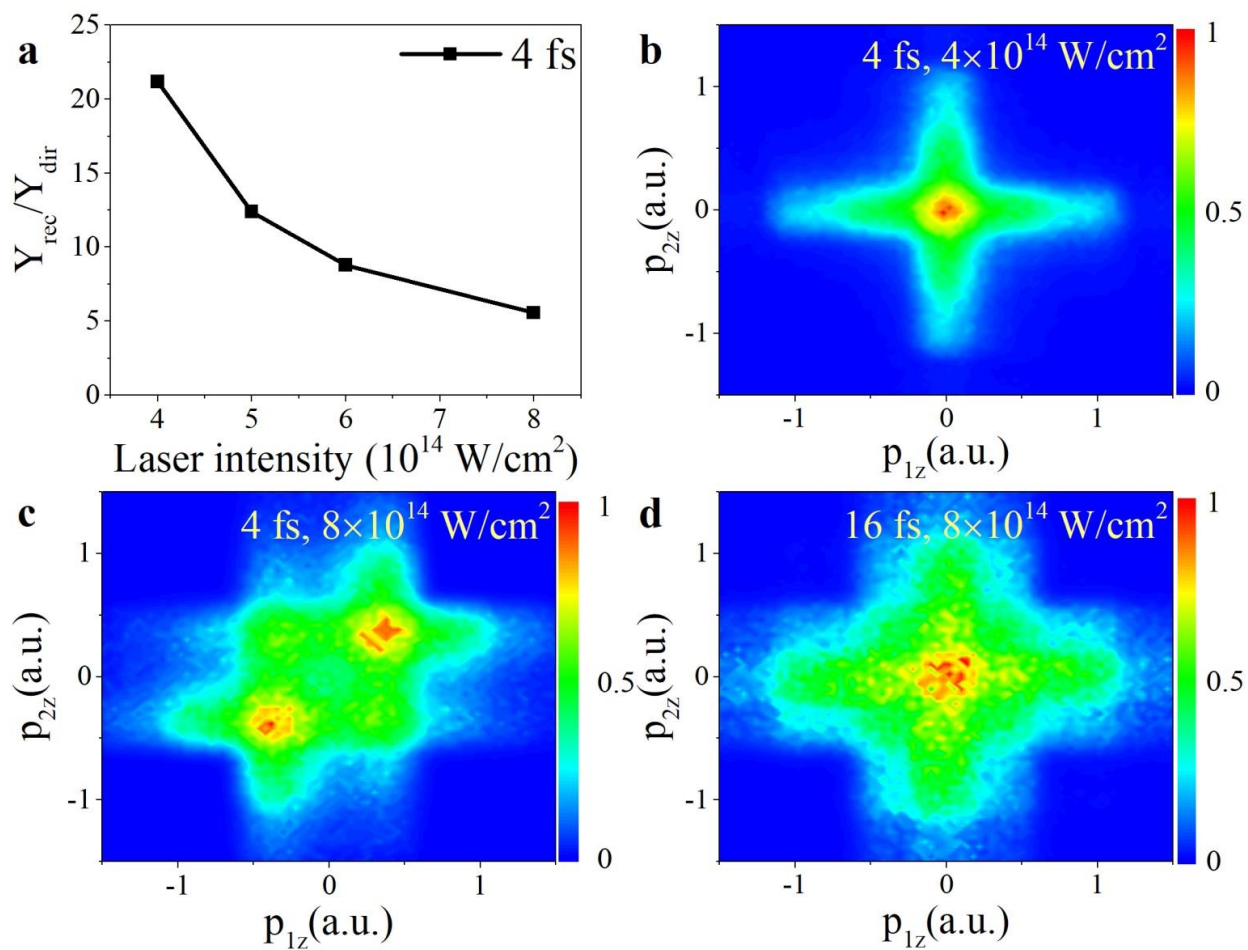
**Fig. 4. Distributions corresponding to the first- and third-return trajectories of  $e_1$ .** (a) CEMDs corresponding to the first return. (b) CEMDs corresponding to the third return. (c) Pulse-duration dependence of  $Y_{3rd}/Y_{1st}$ , the ratio of the integrated yield of the third-return to that of the first-return trajectories of  $e_1$ . The laser intensity is  $1.25 \times 10^{14}$  W/cm<sup>2</sup>. Each CEMD is normalized to itself. The CEPs are averaged.



370

371 **Fig. 5. Effect of Coulomb field of  $\text{Ar}^{2+}$  on CEMDs.** (a) Schematic representation of the laser  
 372 electric field  $\mathbf{E}(t)$  and the corresponding vector potential  $\mathbf{A}(t)$  for pulse duration of 30 fs.  $e_1$   
 373 collides with the ion most probably at the crossing of  $\mathbf{E}(t)$  at  $t_{1r}$  or  $t'_{1r}$ . Upon the collision,  $e_2$  is  
 374 excited, and then is ionized most probably at the peak of the laser field at  $t_{2i}$  or  $t'_{2i}$ . The  
 375 subsequent evolution of the canonical momentum  $p_{2z} - \mathbf{A}(t)$  for the recolliding trajectories of  $e_2$ ,  
 376 denoted as I and II, are presented to illustrate the Coulomb-field effect of  $\text{Ar}^{2+}$ . (b) and (c)  
 377 CEMDs without performing electron indistinguishability symmetrization, and only recolliding  
 378 trajectories of  $e_2$  with ionization time nearest the collision time of  $e_1$  are included. (d) and (e)  
 379 CEMDs calculated by replacing the ionization amplitude  $M_{p_2}^{(3)}$  in Eq. (1) with the standard SFA.

380 Trajectories of  $e_1$  are confined to the first return in (b) and (d), and the third return in (c) and (e).  
 381 Each CEMD is normalized to itself. The CEPs are averaged.



382

383

384

385

**Fig. 6. Simulated results for below-threshold NSDI of  $\text{Ar}^+$  which finally becomes  $\text{Ar}^{3+}$  in 400 nm laser pulse. (a) The ratio between the integrated yields of recolliding and direct trajectories for  $e_2$ . (b)-(d) Normalized CEMDs. The CEPs are averaged.**

## Supplementary Files

This is a list of supplementary files associated with this preprint. Click to download.

- [ccsfaSM210824.doc](#)